AIAA/AAS Astrodynamics Specialist Conference and Exhibit
16 - 19 August 2004, Providence, Rhode Island

AIAA 2004-5211

# Formation Control of the MAXIM $L_2$ Libration Orbit Mission

David Folta* and Kate Hartman#
NASA Goddard Space Flight Center
Greenbelt, MD 20771

Kathleen Howell[a] and Belinda Marchand[b]
School of Aeronautics and Astronautics
Purdue University
West Lafayette, IN 47907

## *Abstract*

The Micro-Arcsecond X-ray Imaging Mission (MAXIM), a proposed concept for the Structure and Evolution of the Universe (SEU) Black Hole Imager mission, is designed to make a ten million-fold improvement in X-ray image clarity of celestial objects by providing better than 0.1 micro-arcsecond imaging. Currently the mission architecture comprises 25 spacecraft, 24 as optics modules and one as the detector, which will form sparse sub-apertures of a grazing incidence X-ray interferometer covering the 0.3-10 keV bandpass. This formation must allow for long duration continuous science observations and also for reconfiguration that permits re-pointing of the formation. To achieve these mission goals, the formation is required to cooperatively point at desired targets. Once pointed, the individual elements of the MAXIM formation must remain stable, maintaining their relative positions and attitudes below a critical threshold. These pointing and formation stability requirements impact the control and design of the formation.

In this paper, we provide analysis of control efforts that are dependent upon the stability and the configuration and dimensions of the MAXIM formation. We emphasize the utilization of natural motions in the Lagrangian regions to minimize the control efforts and we address continuous control via input feedback linearization (IFL). Results provide control cost, configuration options, and capabilities as guidelines for the development of this complex mission.

* Senior Aerospace Engineer, Flight Dynamics Analysis Branch, NASA Goddard Space Flight Center, Greenbelt, MD, 20771, Code 595
#MAXIM Formulation Manager, NASA Goddard Space Flight Center, Greenbelt, MD, 20771, Code 496
[a]Professor, School of Aeronautics and Astronautics, Purdue University, West Lafayette, IN 47907
[b]Graduate Student, School of Aeronautics and Astronautics, Purdue University, West Lafayette, IN 47907



This material is declared a work of the U.S. Government and is not subject to copyright protection in the United States.

## I. Introduction

The MAXIM concept for NASA's Black Hole Imager mission utilizes interferometric techniques at the short wavelengths of X-rays to resolve objects as infinitesimal as the Earth at the center of the Milky Way, the solar disk in another galaxy, and at greater distances yet, the huge black holes that power quasars. While MAXIM's image of a black hole will certainly be one of the new century's most spectacular scientific pictures, it will also address leading questions in black hole research. In order to achieve these high-precision angular resolution images, very long optical baselines are needed. Multiple free-flying spacecraft comprise the sparse aperture providing sufficient collecting area as shown in Figure 1. Other components of the interferometric space system are a combiner spacecraft in some cases and the detector spacecraft.[1,2]

Images are generated through interference patterns gathered from the multiple satellites housing the optical elements that form the aperture. The interference patterns or fringes are observed only if the pathlengths are controlled to great precision (nanometers in some cases). The challenge is to control this pathlength in the presence of environmental and spacecraft disturbances driving the need for active control systems. The sparse aperture array is configurable since the formation of the satellites can change, therefore providing greater sensitivity to a range of angular scales allowing the mission concept to meet a variety of target science goals. The science community realizes the importance of space-based interferometry and the potential for significant scientific breakthroughs. The National Academy of Sciences recommended the development of space-based imaging interferometery in its Decadal Report *Astronomy and Astrophysics in the New Millennium.*

In addition to the Black Hole Imager mission, NASA has several space interferometers planned in the future to explore the universe, image stars, detect gravitational waves, and search for life: Stellar Imager(SI), Submillimeter Probe of the Evolution of Cosmic Structure (SPECS), Space Interferometer Mission (SIM), Terrestrial Planet Finder (TPF), Laser Interferometer Space Antenna (LISA), and Planet Imager. Since several of these missions involve formation flying, research on formation control of space-based interferometers is extremely important to achieving the bold and compelling science waiting to be discovered.

The concept of formation flight of multiple spacecraft near the libration points of the Sun-Earth/Moon (SEM) system offers as many possibilities for space exploration as technical challenges, of which the MAXIM mission is a prime example. MAXIM orbits the $L_2$ Lagrange point and necessitates a very stringent line-of-sight (LOS) pointing that affects the formation control scheme and the overall configuration.[2,3] That is, the alignment of the telescope array LOS (comprised of the separated spacecraft optics and detector) with respect to the target must have stability better than the angular resolution during an observation. In the baseline design, the individual s/c only require a pointing accuracy of 10 arcsec. We must detect spacecraft translations relative to the LOS defined by the target and a fiducial point on one spacecraft. Control of the formation at a micron level is required.

We focus on the dynamics and control of formation flight in a full ephemeris modeling of the libration orbit to incorporate all gravitational perturbations. Solar radiation pressure is also included. A continuous control technique is applied to control the MAXIM formation to the required specifications. The rich natural dynamics near the libration points are explored in depth to aid in the development of more complex formations that meet MAXIM formation requirements. Our analysis focuses on the amount and duration of the formation control effort versus science observation requirements as measured in the formation optics plane.

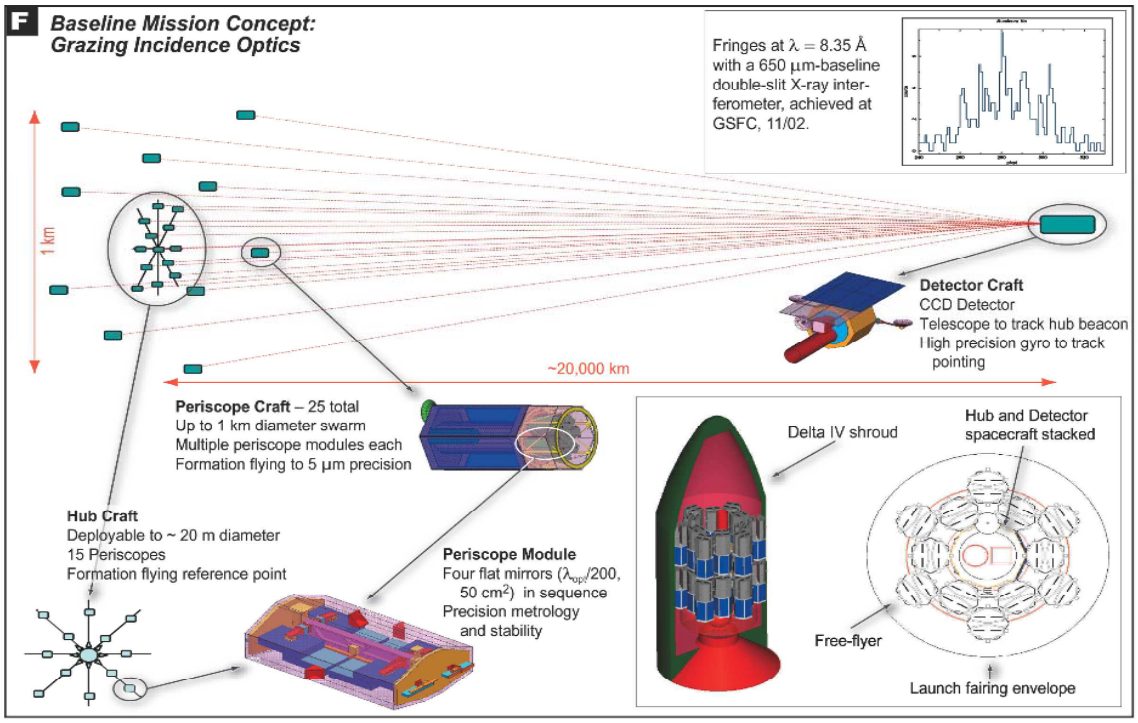


**Figure 1 - MAXIM Baseline Mission Concept using Grazing Incident Optics**

### A. Modeling assumptions

MAXIM is comprised of three formation components; the hub spacecraft, freeflyer (periscope) spacecraft, and the detector spacecraft, which is at a distance of up to 20,000 km from the hub. The spacecraft areas and masses are taken from a GSFC Integrated Mission Design Center design. The wet mass (bus plus payload) for the Hub is 331 kg, the freeflyer spacecraft is 304 kg, and the detector spacecraft is 619 kg. The hub and freeflyers have the same hexagon shape of 1.3 x 2 meters while the detector spacecraft is 1.5 x 1.5 meters but has a varying area depending on its profile (top view is 1.9 $m^2$, side view is 3.3 $m^2$; back/front view is 5.6 $m^2$).

The science observation duration is 1e5 secs and is considered a "typical" exposure time required to image supermassive black holes. The control effort considers requirements for observations with and without thrust accelerations. The controller options for analysis are off during observation durations and on in between to realign and maintain the formation. The other option is continuously on during observations. The control effort emphasizes continuous control but we review a discrete control example as well.

The targets proposed include the Galactic Center, M87, NGC 4594, Cen A, NGC 4258, NGC 3227, NGC 5548, NGC 4151, and MCG-6-30-15. While the selection of the targets may affect the control effort, a mid point of +45 degree elevation and+ 45 degree azimuth as measured in the inertial system was chosen for analysis of the maintenance cost.

The size of the $L_2$ libration orbit used in the analysis is of a typical mission such as the Wilkinson Microwave Anisotropy Probe (WMAP). While the obvious goal is to provide a minimum $\Delta V$ budget for the transfer and injection implying a large Lissajous orbit, the effect on the formation

control is not as pronounced. Solar radiation pressure is included as the spacecraft are not all the same area and mass.

As seen in Figure 1, the hub and freeflyers form a physical configuration defined here as the optics plane which is perpendicular to the detector-hub line of sight (LOS) to a target. The use of the optics plane associates a physical configuration (the states of the freeflyers relative to the hub) to science requirements derived from a Fourier transform of the image plane, the UV plane. The phasing of the mirrors in the freeflyer spacecraft generates a common path length to perform interferometry. Maintaining this optics plane, that is, this physical configuration is our driving requirement for the formation control. During one exposure, the distance of an individual freeflyer from the hub must change by less than 5 microns, so the light contributed by each freeflyer to the image moves by less than the width of the point spread function. What is important here is that motions of more than 5 microns translate into a change in optical path length for that channel of more than 1/10th of a wavelength. The MAXIM formation specifies that 25 spacecraft are to be used. Our preliminary analysis uses the detector, the hub, and six freeflyers at the maximum nominal radial distance of 500 meters from the hub in the optics plane. The current science concept achieves the required angular resolution of 0.05 micro-arcseconds with an effective collecting area of 1,000 $cm^2$. This is done by distributing the periscope mirrors among the 25 formation flying spacecraft, across a virtual aperture of one kilometer diameter with focal length of 20,000 km and 5 micron pixel size.

The separation between the detector and the hub is also important. For our analysis we used the largest distance specified of 20,000 km. For the smaller separation of 200 km, the hub and freeflyers would be 'attached', yielding a completely different control effort. A minimal thrust level of one μN poses some current technology challenges but may be required to meet the assumptions and requirements.

### B. MAXIM Libration Orbit

The nominal orbit used in our analysis places the hub spacecraft on a reference that evolves along an $L_2$ Halo orbit that has amplitudes of 700,000 km in $A_Y$ and 200,000 km in $A_Z$. The reference Halo orbit was computed with a full Ephemeris model and is shown in Figure 2. Six freeflyers are evenly spaced, each at 500-meter distance from hub, on the optics plane. The detector spacecraft is 20,000 km aft of the hub, along the –W direction as seen in Figure 3. The target is at +45 deg azimuth and +45 deg elevation relative to EMEJ2000 Inertial Frame. Solar Radiation Pressure (SRP) effects based on equal effective areas for each spacecraft (2.0106e-6 $km^2$) are used. Previous analysis demonstrated that the ΔV cost for

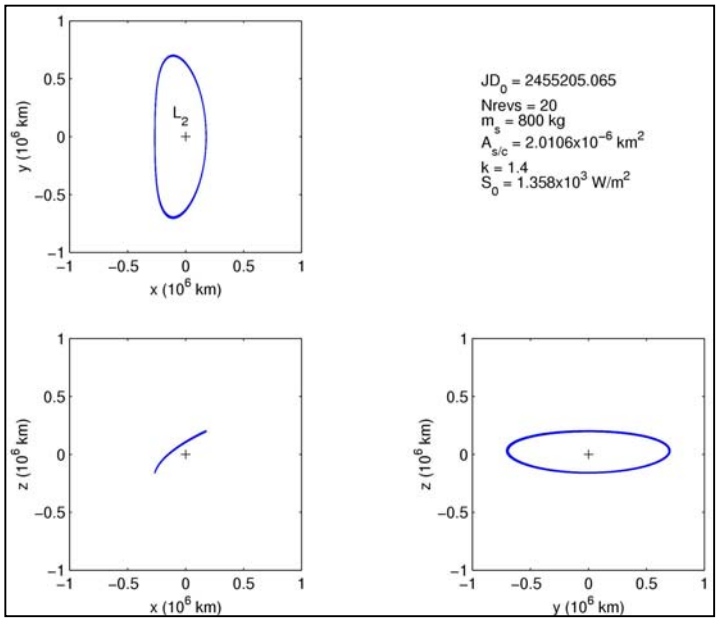


**Figure 2. MAXIM L2 Halo Orbit with Ay = 700,000 km and Az = 200.000km**

formation maintenance varies over the orbit as a function of the elevation and azimuth angles.[5] The target angle represents a location that is neither a worst case nor best case for the ΔV cost to maintain the direction.

### C. MAXIM Frame Definition

The definition of the frame used for our control is shown in Figure 4. The X, Y, Z axes show the ephemeris inertial axes and the local frame is represented by u, v, w. The MAXIM hub spacecraft is located at the X,Y,Z origin and the angles α, δ provide the alignment toward the target. The target LOS is parallel to the w axis. The alignment is from the detector to the Hub to the target.

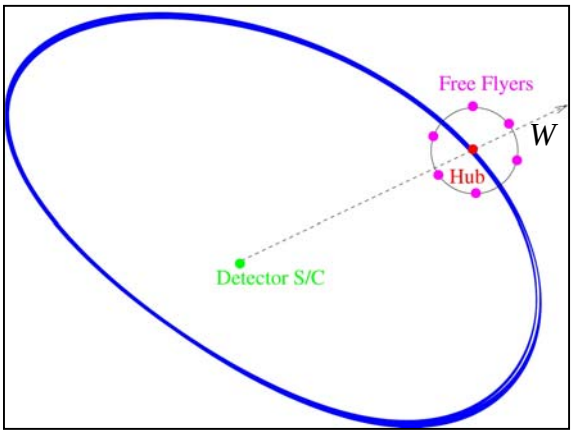


**Figure 3. Orientation Of Hub On Reference Halo Orbit and Freeflyer Alignment (not to scale)**

The local frame components are constructed from the following direction cosines as

$$\hat{w} = C_\alpha C_\delta \hat{X} + S_\alpha C_\delta \hat{Y} + S_\delta \hat{Z}$$

$$\hat{u} = \frac{\hat{Z} \times \hat{w}}{\left| \hat{Z} \times \hat{w} \right|}$$

$$\hat{v} = \hat{w} \times \hat{u}$$

Where the direction cosine matrix (where C=cosine and S = sine) can be constructed as

$${}^{I}C^{U} = \begin{bmatrix} -S_\alpha & -C_\alpha S_\delta & C_\alpha C_\delta \\ C_\alpha & -S_\alpha S_\delta & S_\alpha C_\delta \\ 0 & C_\delta & S_\delta \end{bmatrix}$$

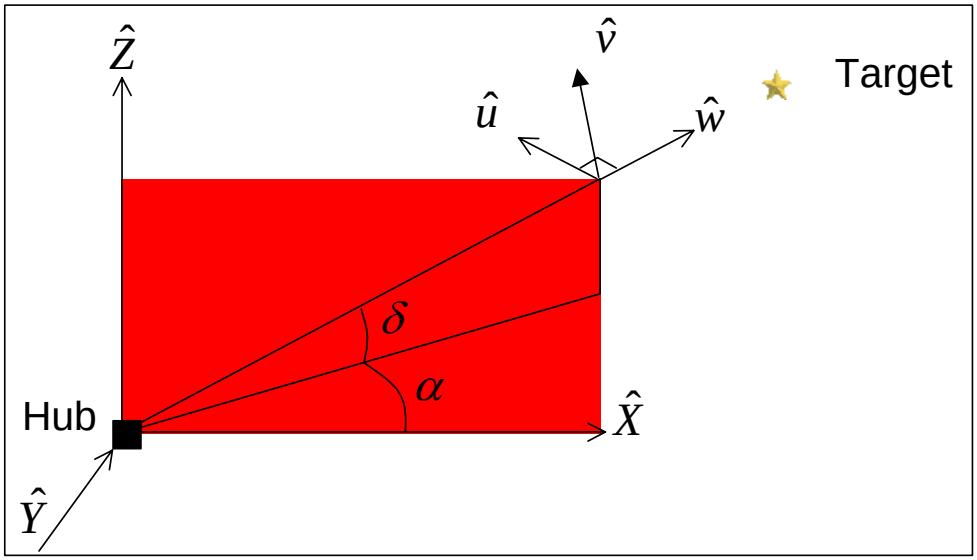


**Figure 4. Maxim Definition for the Inertial (X,Y,Z) and Optics Frames (u,v,w)**

## II. Orbit Control Strategies

Our investigation takes a global view of the large-scale formation flying problem. Much of the research to date considers the continuous control of constellations, clusters, and formations for missions near the Earth, or where the influence of other gravitational perturbations can be safely ignored.[4,7] Impulsive schemes have also been implemented but these only apply to formations that do not require close tracking of a reference solution.[8] Nonlinear methods, combined with adaptive control, have also been developed in the two-body problem.[9,10] In contrast, the documented research on formation flight in multi-body systems is scarce. Most of these investigations focus on the simplified circular restricted three-body problem (CR3BP).[11,12] Some authors do consider formation flight relative to Lissajous trajectories developed in the ephemeris model but the effectiveness of such a controller is only demonstrated relative to the linear dynamics, not the full nonlinear system. That is, the evolution of the controlled formation is not numerically integrated in the nonlinear system but rather approximated from the linear dynamics of the integrated Lissajous trajectory.

Previous work by Howell and Barden and others considered naturally occurring formations derived from center manifold analysis, as well as a discrete impulsive control approach to maintain a prescribed formation plane formed by multiple spacecraft.[11,13-22] One item of interest, which pertains to the continuous control approach, is to obtain a rough analytical approximation of this center manifold motion and determine how continuous optimal control and exact feedback linearization compares, in terms of cost, to the discrete station-keeping approach.[21,22] These works also demonstrate the efficiency and cost effectiveness of both input feedback linearization (IFL) and output feedback linearization (OFL) methods for formation control in the CR3BP. The IFL controller is designed to force the error dynamics of each state variable to follow a critically damped response. The OFL controller, on the other hand, was only initially designed to force the radial separation between each spacecraft to track some specific value. Hence, no relative orientation requirements were imposed on the formation. But, the OFL controller can also constrain the orientation rate and that may be beneficial in certain applications. A linear quadratic regulator (LQR), derived from optimal control theory, yields essentially an identical error response and control acceleration history as the input feedback linearization approach. However, the IFL controller is computationally much less intensive and, by comparison, conceptually simple. We address the properties of the IFL controller in defining the MAXIM formation control.

Our analysis considers strategies to maintain a planar formation of the spacecraft in an orbit about the Sun-Earth $L_2$ point. That is, controlling the deviations of each spacecraft relative to the initial formation plane. For a comparison, a discrete stationkeeping control approach is devised to force the orientation of the formation plane to remain fixed inertially.

### A. Discrete or IFL Control

Even if the onboard propulsion system can deliver an accurate continuous thrust level, it is likely that the science requirements of the mission may stipulate some thruster down-time. This leads then to a new consideration about the degree of accuracy to which the formation can be maintained via discrete impulses applied at the beginning of each N segments. A simple targeter applying discrete impulses can maintain orientation. Alternatively, an LQR controller, based on a discrete time system, yields the optimal magnitude of each differential control impulse at the specified time interval. However, in either case, the nominal control input that must be added is

still assumed to be available as needed. If a continuous nominal control effort is not available, how often must impulsive maneuvers be implemented to maintain the nominal configuration?

Of the two options mentioned here, the most straightforward approach is a simple strategy that targets the state vector at the end of each specified interval. Consider a case of a 100 km formation of two spacecraft, constrained to remain aligned with the inertial *y*-axis at all times. In the absence of any external perturbations, a continuous control approach via IFL requires 0.3348 m/sec of total $\Delta V$ over a period of 180 days. How much will the formation diverge if the control effort is discretized over a period of hours, or even days? Consider the general form of the solution to the linear system,

$$\begin{bmatrix} \delta\bar{r}_1 \\ \delta\bar{v}_1^- \end{bmatrix} = \Phi(t_1, t_0) \begin{bmatrix} \delta\bar{r}_0 \\ \delta\bar{v}_0^+ \end{bmatrix} = \begin{bmatrix} A & B \\ C & D \end{bmatrix} \begin{bmatrix} \delta\bar{r}_0 \\ \delta\bar{v}_0^- + \Delta\bar{v}_0 \end{bmatrix}$$

where $\Phi(t_1, t_0)$ denotes the state transition matrix associated with the nominal Lissajous orbit along which the MAXIM detector spacecraft is assumed to evolve. The symbol $\delta$ denotes a perturbation relative to the nominal Lissajous trajectory and $\Delta\bar{v}_0$ represents an impulsive maneuver applied at the beginning of a segment. The superscripts identify velocity perturbations before and after a maneuver. Controlling the position of the formation spacecraft relative to the detector or hub to a constant vector, as observed in the inertial frame, is equivalent to targeting a particular constant perturbation $\delta\bar{r}_1$ relative to the inertial frame. An impulsive maneuver of the form

$$\Delta\bar{v}_0 = B^{-1}\left(\delta\bar{r}_1 - A\delta\bar{r}_0\right) - \delta\bar{v}_0^-$$

will accomplish the goal in the linear system. A precise implementation of this scheme in the nonlinear system requires that the maneuvers be differentially corrected over each segment. However, the simple expression is found to accomplish the goal, provided the length of each segment is sufficiently small.

A discrete optimal control strategy was also developed and applied to this problem and was formulated to implement impulsive maneuvers at the beginning of each segment. The cost function was defined as the sum of two terms. The first term was a weighted (W) quadratic function of the state errors at the end state; the second term is a weighted (Q) quadratic function of the state deviations along the path. Of course, the simple corrector only targets the states at the end of each segment so the deviations of the six states along the path will be greatest with a discrete set of impulses determined via such a targeting scheme. Along the path, the optimal controller was formulated to weight position deviations to be twice as costly as velocity state errors. Then, the end-state weighting can be varied.

Not surprisingly, the total $\Delta V$ computed via either discrete control approach converges on the cost computed via the continuous control approach as the interval between maneuvers becomes shorter. The state corrector only targets position, not velocity. Hence, the rate of divergence is increased because the velocity error at the terminal point of each segment is not zero. This position divergence appears for a MAXIM example in Figure 5 for a sampling of three distinct discrete controllers. The dashed red line in the figure is a simple targeter. At a given time, an impulse targets the required position at a time in the future, in this case 6 days. The plot shows the position deviations between maneuvers. Note that if we cut the time interval in half, we will cut the deviations in half. The blue is a discrete optimal controller that minimized the state deviations without end point weighting. (Note that the largest amplitude points along the blue

curve correspond to the impulses.) This optimal controller does cut the state error between maneuvers. The green line is generated as a discrete optimal controller but with an increase in the weighting on the end state ($Q_m$ = $1e^{-2}$ Q). The deviations naturally increased. If the end-state weighting increases a sufficient amount, the deviations are the same as the simple targeter. Actually there is a fourth curve in the figure. A magenta curve is plotted for the optimal controller with a large weighting on the end states. It is, in fact, seemingly identical in the figure to the red curve produced with the simple targeter. In any case, once the spacecraft reaches the target position it will move away from it because the relative velocity is not zero. Note that the deviation is in meters and implies that to meet the MAXIM requirements, the discrete control would need to run near continuously. An interval of only a few seconds is available before the constraints are violated. This leads us to use a true continuous controller, that is, the input feedback linearization method.

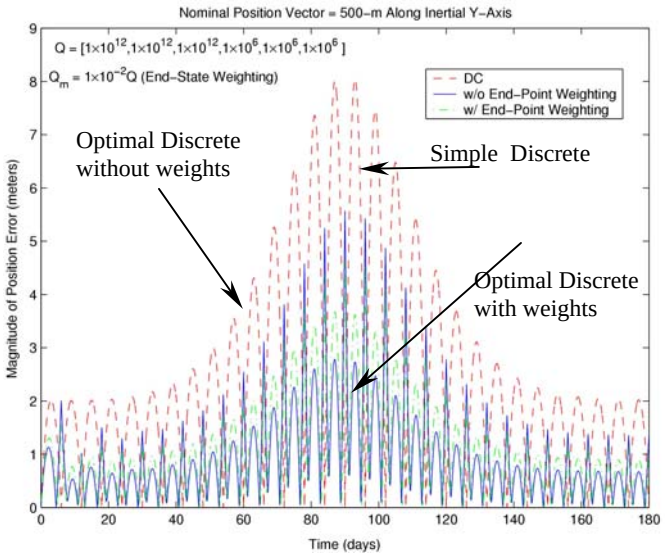


**Figure 5. MAXIM Position Deviation with Discrete Control with Maneuvers Every Six Days**

In general, the control goal should seek to minimize the integral of the error while only resorting to discretized maneuvers, which ensures that the overall error is minimized everywhere along the segment rather than at the endpoints alone. This minimization is one of the issues to be further addressed in this continuing investigation. Another aspect of this study considers the robustness of these control strategies in the presence of modeling uncertainties.

### B. Control Methodology

It was first thought that the control methodology might be based on the use of a paraboloid as a control surface for the freeflyers as shown in Figure 6.[19] Here the hub is located at the center of the paraboloid and the parabola shape constrains the freeflyer spacecraft. This geometric shape allows for a controller that can accommodate freeflyers at various radii and has been used successfully to shift freeflyers from one radius to another. When the problem is formulated in

$$\tilde{x} = a_p \sqrt{u_p / h_p}\cos\nu$$
$$\tilde{y} = a_p \sqrt{u_p / h_p}\sin\nu$$
$$\tilde{z} = u_p + q$$
$$\bar{r}_E^{\,HD_i} = \tilde{x}\hat{u} + \tilde{y}\hat{v} + \tilde{z}\hat{w}$$

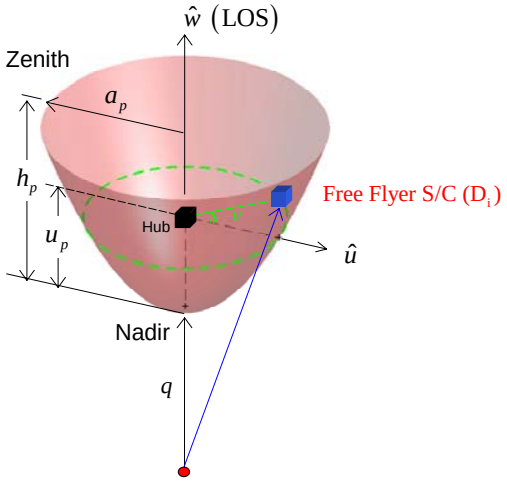


**Figure 6. Possible Parabolic Configuration Concept**

terms of the paraboloid variables $(q, \nu, u)$, however, the controller is not designed for cases when the detector or any of the freeflyers are along the line of sight. The difficulty is a singularity in this geometry. In this configuration, the freeflyers (deputy spacecraft) are placed on the dashed green line and evenly spaced. Thus, alternatively, the control problem is formulated in Cartesian coordinates that are related to the paraboloid variables as needed.

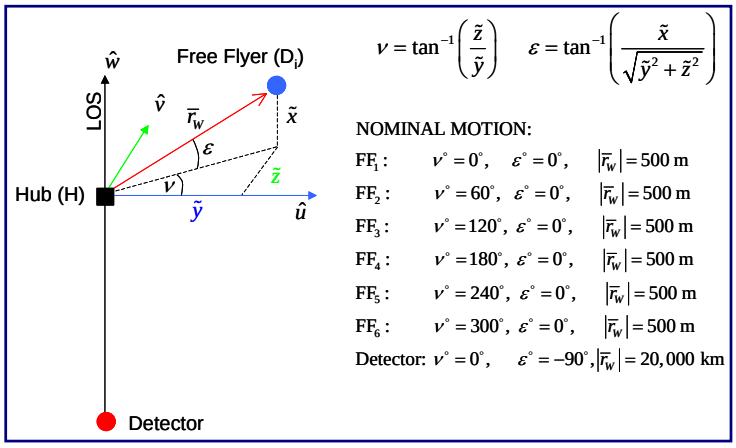


**Figure 7 Nominal Motion and Determination of Vehicle Position Relative to UVW-Frame**

This formulation can be modified to the configuration shown in Figure 7 where the angle ν is the parameter of importance for science observations. In Figure 7, the nominal behavior would correspond to ε = 0. The angle ν is measured in a counterclockwise direction (similar to azimuth) Each freeflyer has its own $\hat{d}_1$ and the kinematics are written as

$$\bar{r}^{HD_i} = r\hat{d}_1$$
$$^{U}\dot{\bar{r}}^{HD_i} = \dot{r}\hat{d}_1 + r\dot{\nu}C_\varepsilon\hat{d}_2 + r\dot{\varepsilon}\hat{d}_3$$
$$\hat{d}_1 = C_\varepsilon C_\nu\hat{u} + C_\varepsilon S_\nu\hat{v} + S_\varepsilon\hat{w}$$

We define a conservative displacement tolerance in ν and $\hat{d}_1$ of 5-microns. Each freeflyer is at a given nominal orientation with respect to the hub with a value of ν and ε. To relate the Cartesian coordinates to spherical,

$$\tilde{x} = rC_\nu C_\varepsilon \qquad \dot{\tilde{x}} = \dot{r}C_\nu C_\varepsilon - r\dot{\nu}S_\nu C_\varepsilon - r\dot{\varepsilon}C_\nu S_\varepsilon$$
$$\tilde{y} = rS_\nu C_\varepsilon \qquad \dot{\tilde{y}} = \dot{r}S_\nu C_\varepsilon + r\dot{\nu}C_\nu C_\varepsilon - r\dot{\varepsilon}S_\nu S_\varepsilon$$
$$\tilde{z} = rS_\varepsilon \qquad \dot{\tilde{z}} = \dot{r}S_\varepsilon + r\dot{\varepsilon}C_\varepsilon$$

The nominal motion is in the spherical coordinates while the control effort is formulated in the inertial focal frame. Using initial conditions of a 1 km diameter plane for the freeflyer spacecraft, the formation is defined in terms of the spherical coordinates as follows. For this example, it is easily translated into the Cartesian coordinates. Note again that these are components in and normal to the optics plane.

$$\left.\begin{array}{ll} r = 20{,}000 \text{ km} & \dot{\tilde{x}}^* = 0 \\ \nu = 0 & \dot{\tilde{y}}^* = 0 \\ \varepsilon = -\pi/2 & \dot{\tilde{z}}^* = 0 \end{array}\right\} \quad \left.\begin{array}{ll} \tilde{x}^* = r^* C_\varepsilon & \dot{r} = 0 \\ \tilde{y}^* = 0 & \dot{\nu} = 0 \\ \tilde{z}^* = r^* S_\varepsilon & \dot{\varepsilon} = 0 \end{array}\right.$$

$$\left.\begin{array}{ll} r^* = 1 \text{ km} & \dot{r}^* = 0 \\ \nu^* = n\pi/3; (n = 0 \ldots 5) & \dot{\nu}^* = 0 \\ \varepsilon^* = 0 & \dot{\varepsilon}^* = 0 \end{array}\right\} \quad \left.\begin{array}{ll} \tilde{x}^* = r^* C_{\nu^*} & \dot{\tilde{x}}^* = 0 \\ \tilde{y}^* = r^* S_{\nu^*} & \dot{\tilde{y}}^* = 0 \\ \tilde{z}^* = 0 & \dot{\tilde{z}}^* = 0 \end{array}\right.$$

### C. Controller Development [20-22]

The controlled equations of motion (EOM) in the ephemeris frame (as related to an Earth centered frame) are expressed where $P_2$ is the Earth. Here "D" can be representative of either the deputy (freeflyer) or the detector in terms of using the equation for control. The superscript on the left denotes the frame used for formulation of the differential equations.

$$ {}^{I}\ddot{\bar{r}}_I^{P_2D_i} = \bar{f}\left(\bar{r}_I^{P_2D_i}, {}^{I}\dot{\bar{r}}_I^{P_2D_i}\right) + \bar{u}_I^{(D_i)}(t) $$

$$ {}^{I}\ddot{\bar{r}}_I^{P_2H} = \bar{f}\left(\bar{r}_I^{P_2H}, {}^{I}\dot{\bar{r}}_I^{P_2H}\right) $$

Since the hub is assumed to move in a Lissajous orbit computed in a full ephemeris model, no control is included for its evolution along this path. The controller is selected to the type of response that is required, and in most cases this is a critically converging system. The above terms are subtracted to yield the EOM for the relative motion in both the inertial and the u,v,w frame by using the direction cosine matrix for rotation into the focal plane. The controller in the local frame is constructed as follows,

$$ {}^{U}\ddot{\bar{r}}_U^{HD_i} = \left\{{}^{U}C^{I}\right\}\Delta\bar{f}_I + \left\{{}^{U}C^{I}\right\}\bar{u}_I^{(D_i)}(t) = \left\{{}^{U}C^{I}\right\}\Delta\bar{f}_I + \tilde{u}^{(D_i)}(t) $$

Here the dynamics of the system can be annihilated by the first term in the IFL controller and the remaining terms show the critical response chosen for the IFL controller.

$$ \tilde{u}^{(D_i)}(t) = -\left\{{}^{U}C^{I}\right\}\Delta\bar{f}_I^{(D_i)} - 2\omega_n\left({}^{U}\dot{\bar{r}}_U^{HD_i} - \dot{\bar{r}}^{*}\right) - \omega_n{}^{2}\left(\bar{r}_U^{HD_i} - \bar{r}^{*}\right) $$

$$ {}^{I}\ddot{\bar{r}}_I^{HD_i} = \Delta\bar{f}_I + \bar{u}_I^{(D_i)}(t) \quad \rightarrow \quad \left\{{}^{I}C^{U}\right\}{}^{U}\ddot{\bar{r}}_U^{HD_i} = \Delta\bar{f}_I + \bar{u}_I^{(D_i)}(t) $$

Once the control is determined in the optics frame to generate a critical response, it is translated back into the inertial frame for use by the control algorithm,

$$ \bar{u}_I^{(D_i)}(t) = \left\{{}^{I}C^{U}\right\}\tilde{u}^{(D_i)}(t) $$

It is assumed that this control is available continuously.

## III. RESULTS

Figure 8 shows the orientation of a sample MAXIM formation. The left view is the optics plane view and the arbitrary positions of the six freeflyers relative to the hub. On the right is the inertial frame view. The cost over one revolution of a halo or Lissajous for each freeflyer and the detector is slightly different for each but generally similar. In these cases the solar radiation pressure is turned on. An effective area of $1.6\text{m}^2$ is assumed.

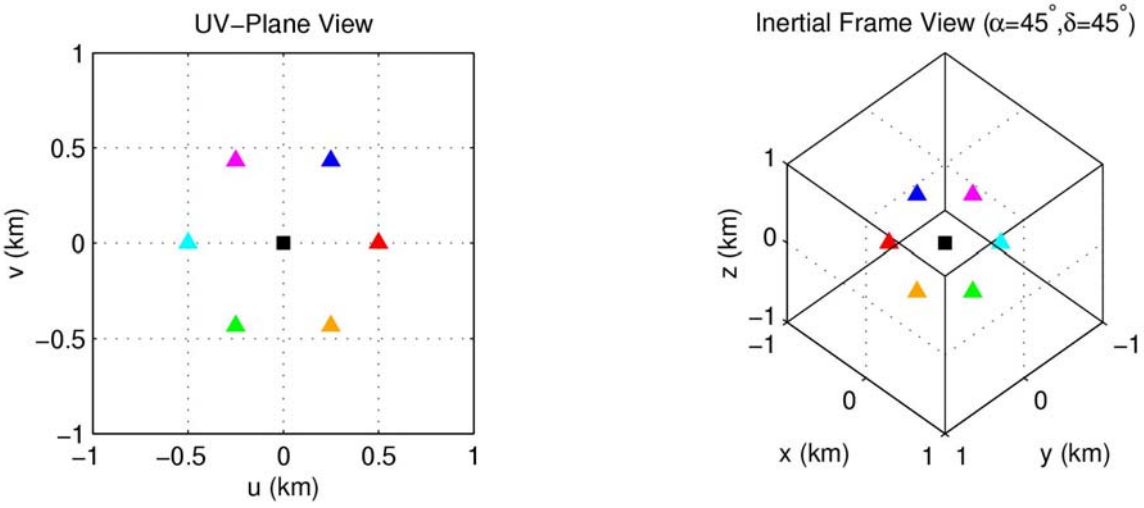


**Figure 8. MAXIM formation design for IFL control**

### A. Maintenance Maneuvers

Maintenance maneuvers must be performed during the mission to preserve the strict separation and orientation requirements. Using IFL, a control effort for 180 days (one libration orbit revolution) was computed and shown in Figure 9 are the thrust profiles for both the detector and the freeflyer spacecraft. The effort is on the order of several mN for the detector and tenths of μN

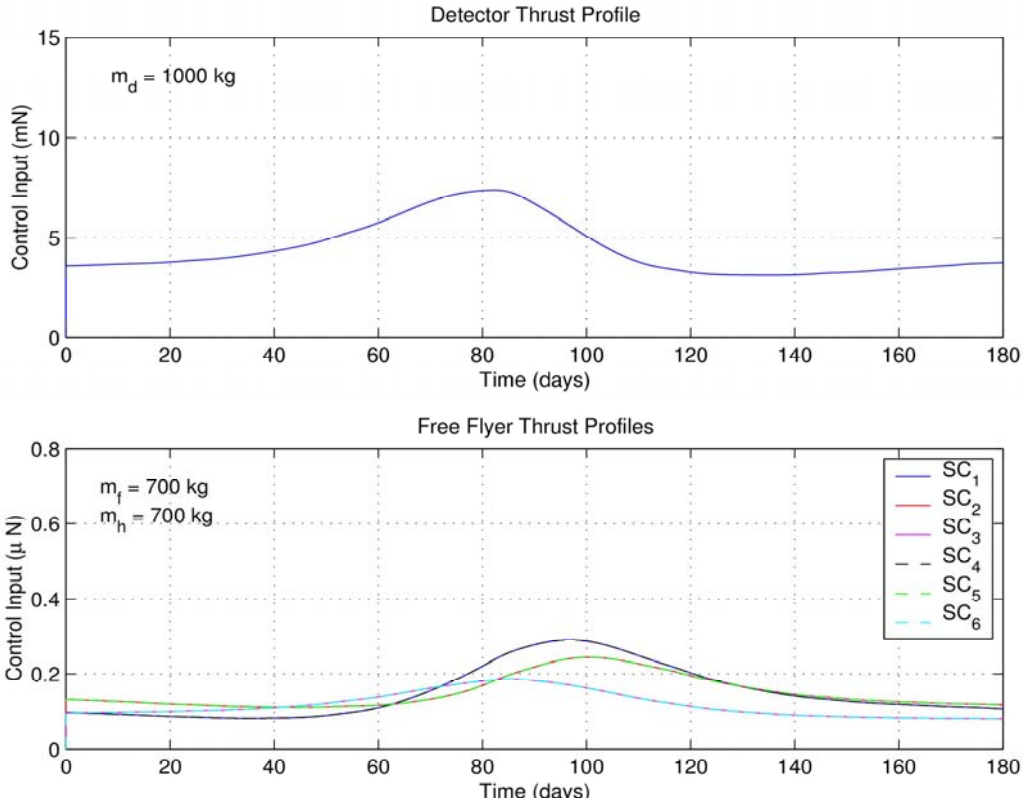


**Figure 9. 180 Day Thrust Profile for Continuous IFL Control**

for the freeflyers. If the mass ratios are changed, doubling the mass, the thrust profile changes accordingly requiring twice as much thrust as shown in Figure 10.

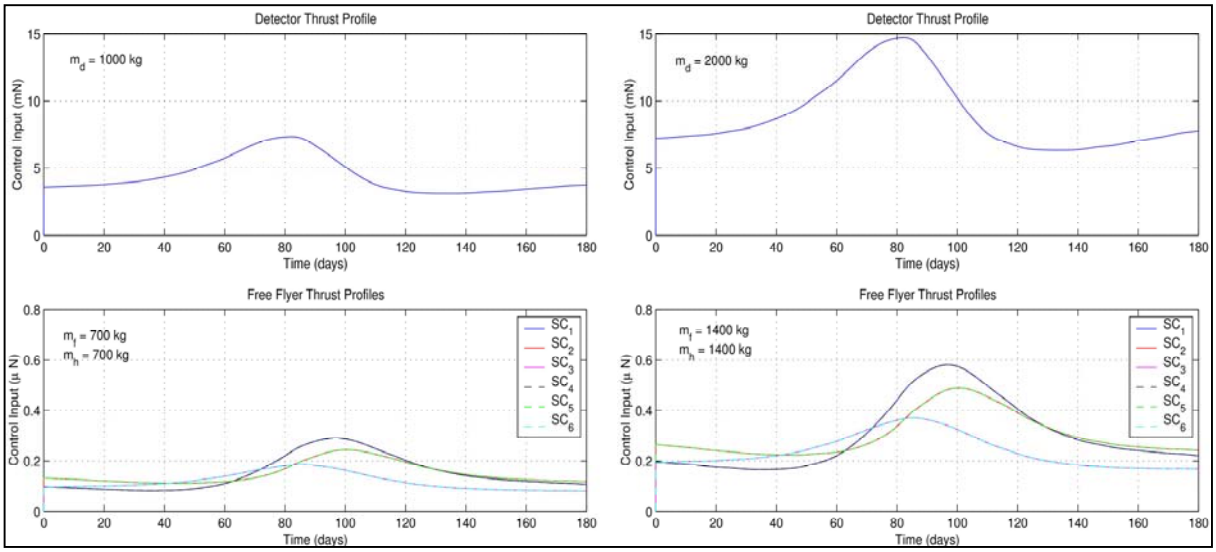


**Figure 10. Variation in Thrust Profile for Select Mass Ratios**

## B. Maintenance and Recovery

We considered the effect on turning the thrusters off during a MAXIM observation, which is 100,000 seconds long in duration. This was done to analyze any requirement of eliminating accelerations from the small but continuous maintenance. This also allowed us to investigate the drift in the formation over a small time period and to establish the thrust profile necessary to recover the original formation alignment. Figure 11 shows the increase in radial errors of the detector and the freeflyers with respect to the hub over the observation duration. Once the 100,000 seconds is reached, the controller is activated again to reset the freeflyer and detector for

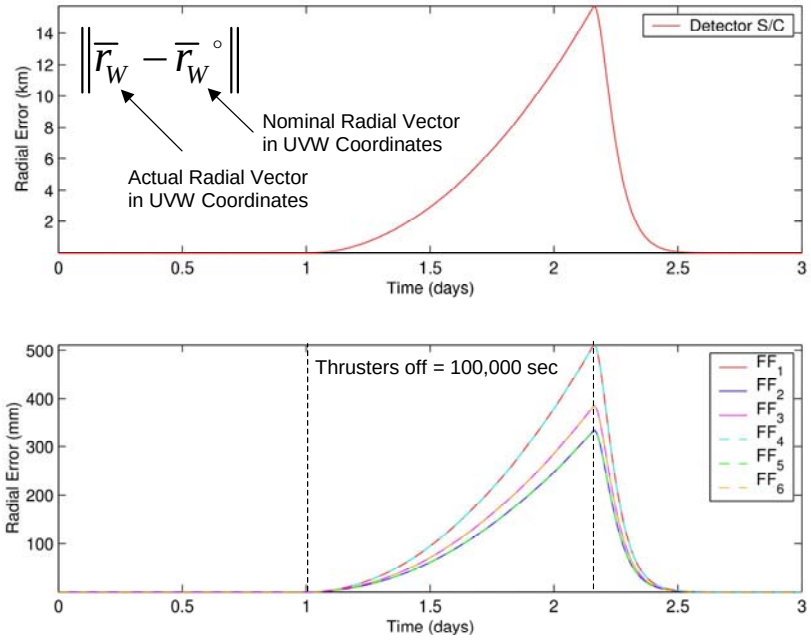


**Figure 11. Radial Error During No Control**

the nominal configuration, without any error. Note that the errors are not linear and ramp up in the typical exponential fashion for a libration orbit. The peak radial error of 15 km was observed for the detector at a distance of 20,000 km from the hub. The freeflyer radial errors were smaller, ranging from 300 mm to 550 mm. Figures 12 and 13 show the errors in the optics frame (u,v,w) components. Also apparent is the in-plane (u and v components) and out-of-plane deviation. Figure 14 shows these errors as pointing errors in arc-seconds. The formation requirements for the freeflyers includes a radial error in the optics plane of less than five microns, clearly less than 1mm, and an azimuthal angle error (ν-ν*) less than 5 micro-arcseconds. One can easily see that the drift results in the science requirements being violated. It is also apparent that the radial error exceeds the requirement very quickly and shortening the duration is not a feasible solution.

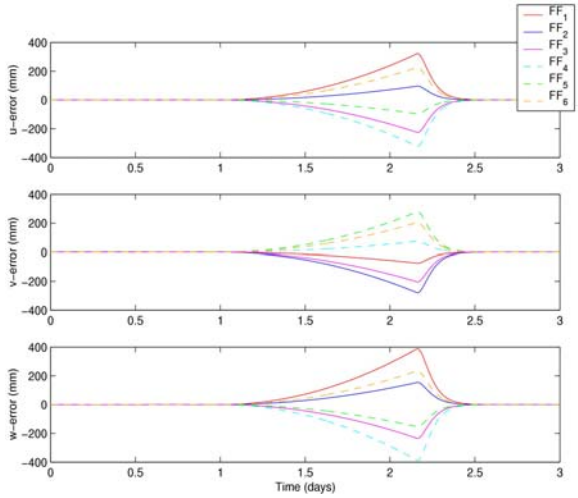


**Figure 12. Freeflyer Focal Plane Error (u,v,w) during No Control**

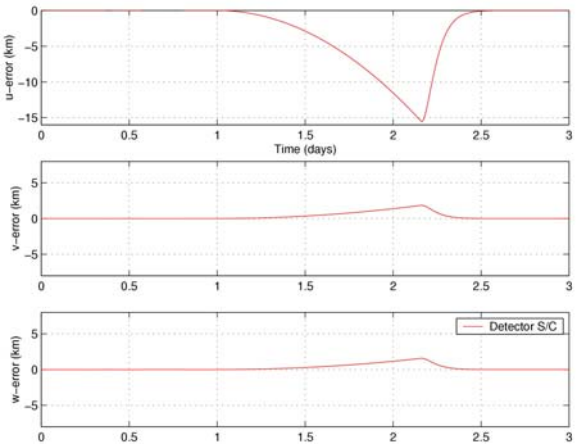


**Figure 13. Detector Focal Plane Error**

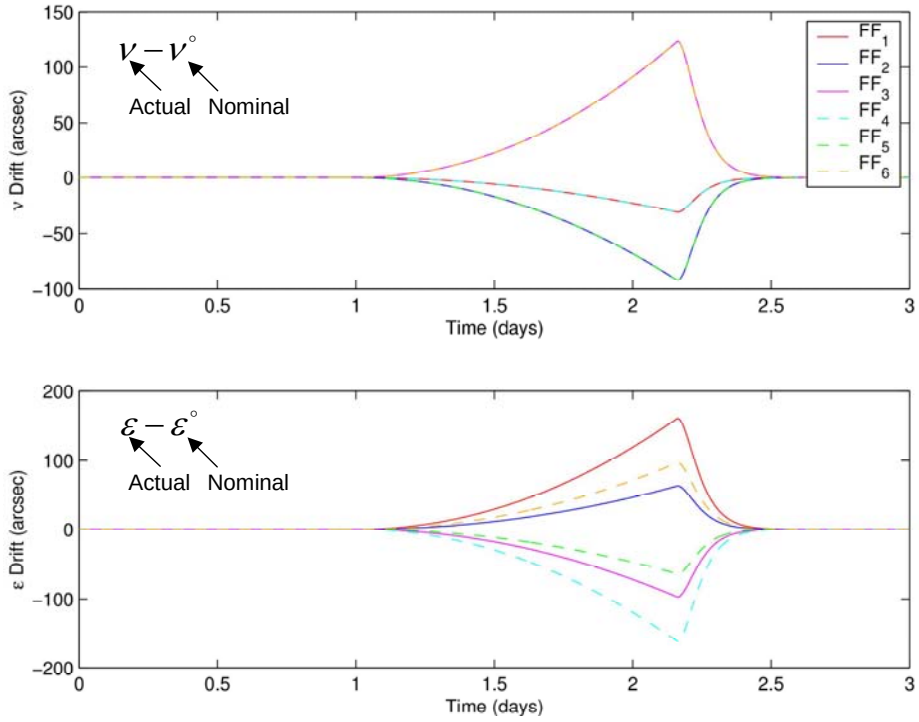


**Figure 14. Freeflyer Focal Plane Error in Arcseconds**

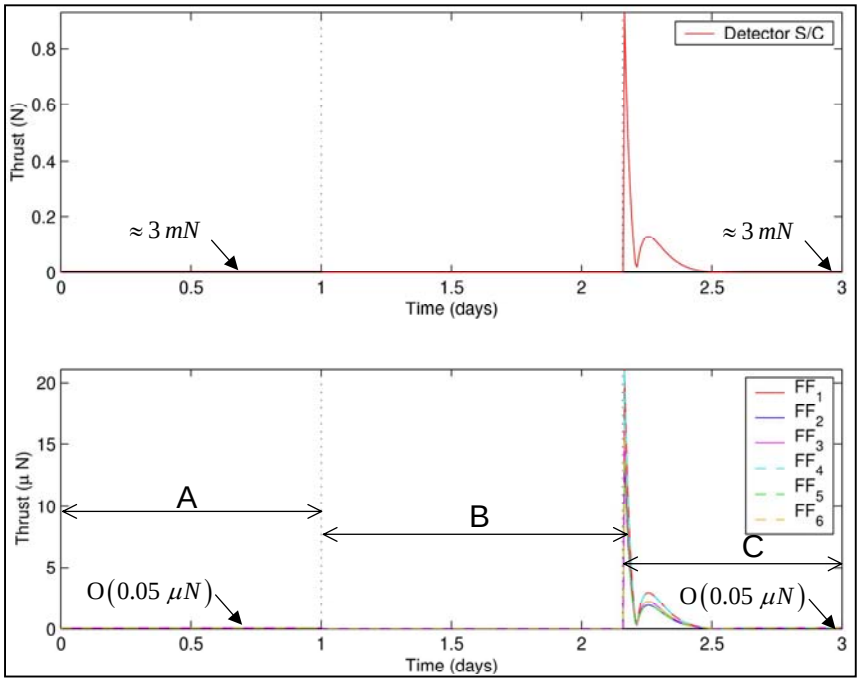


**Figure 15. Three Day Span with Maintenance, No Control, and Recovery**

To assess the thrust level and compare on-off thrust magnitude, Figure 15 shows the thrust profile for the detector and freeflyers during a three day span that includes 1 day of maintenance, 100,000 seconds of no-control due to science observations, and the recovery over less than ½ day. The recovery thrust levels reached one N for the detector (top plot) while the freeflyers (bottom plot) required less than 10 μN. Figure 16 shows the thrust profile for the maintenance (segment A) of the 3-day simulation. The detector control required 3e-3 N while the freeflyers required less than 0.05 μN. During maintenance the scale of the plot implies that the thrust level is constant. In reality, even though the control offsets the perturbations to produce zero error, the thrust level varies because the forces are not constant. This will be more apparent when errors are added to the model. During observation, i.e., no control (segment B) appears as expected and the thrust profile is zero. The recovery thrust profile corresponding to segment C appears in Figure 17.

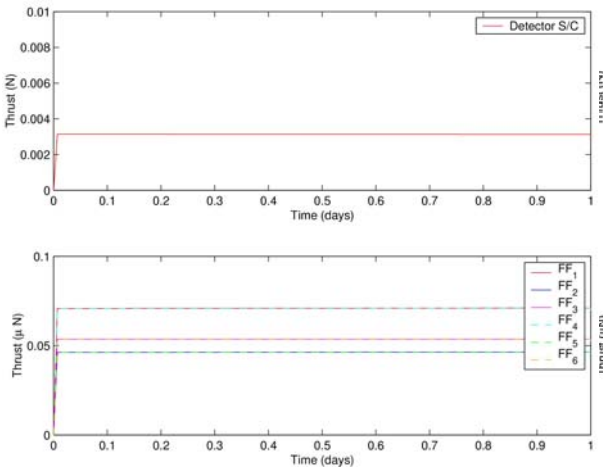


**Figure 16. Maintenance Thrust Profile for Segment A**

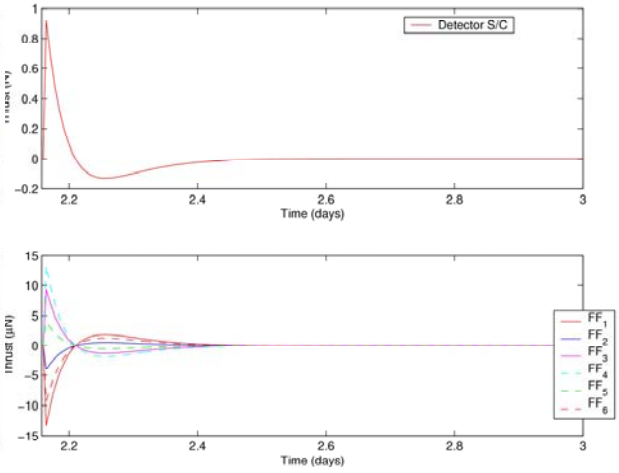


**Figure 17. Recovery Thrust Profile for Segment C**

### C. Reorientation

Another important aspect of the mission is reorientation. In this preliminary investigation, it was also of interest to determine the ability to reorient and the relative cost for a simple scenario. This simple scenario also avoids any consideration of collisions at this time. Reorientation of the formation to view additional targets was accomplished by performing a 90-degree rotation about the inertial z-axis as shown in Figure 18. Initially, the target was assumed to be along the inertial

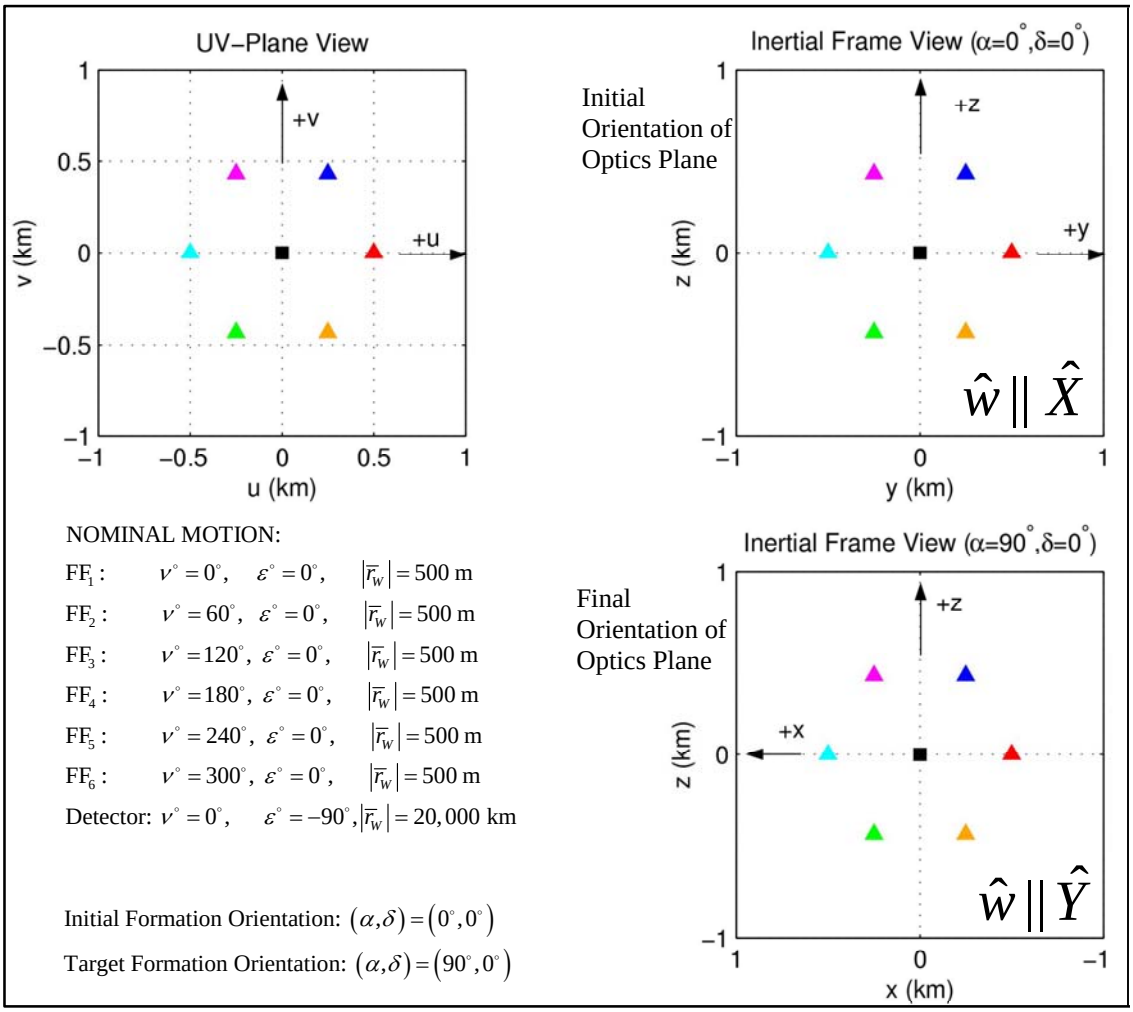


**Figure 18. Formation Reorientation, 90 Degree Change in X-Y plane**

position x-direction. This x-axis pointing was then re-aligned to the y-axis. The elevation angle was held to zero degrees. As seen in Figure 18, the initial to final orientation shows the switch in the direction of the axes with respect to the freeflyer spacecraft. The initial nominal angle information for ν and ε for this sequence is shown in the bottom left.

The thrust levels for the detector and the freeflyer are plotted in Figure 19 over the duration of the reorientation. The thrust profile for the reorientation was allowed a duration of 7 days to minimize the effort of the controller for the detector spacecraft. Even with this amount of time the detector thrust level reached a maximum of 1.5 N and took approximately 8 days to completely recover and settle into the proper configuration. Of course, in this example, the

detector is 20,000 km away. The thrust profile for the freeflyers was much lower at values less than 25μN. Note the secondary increase in the thrust magnitude. This is an artifact of the control as the thrust compensates for the velocities that must also be attained for the proper final state vector of each spacecraft. In Figure 20, the reconfiguration is represented in ephemeris inertial coordinates. Note the switch in the x and y components that show the repositioning of the spacecraft for the reorientation.

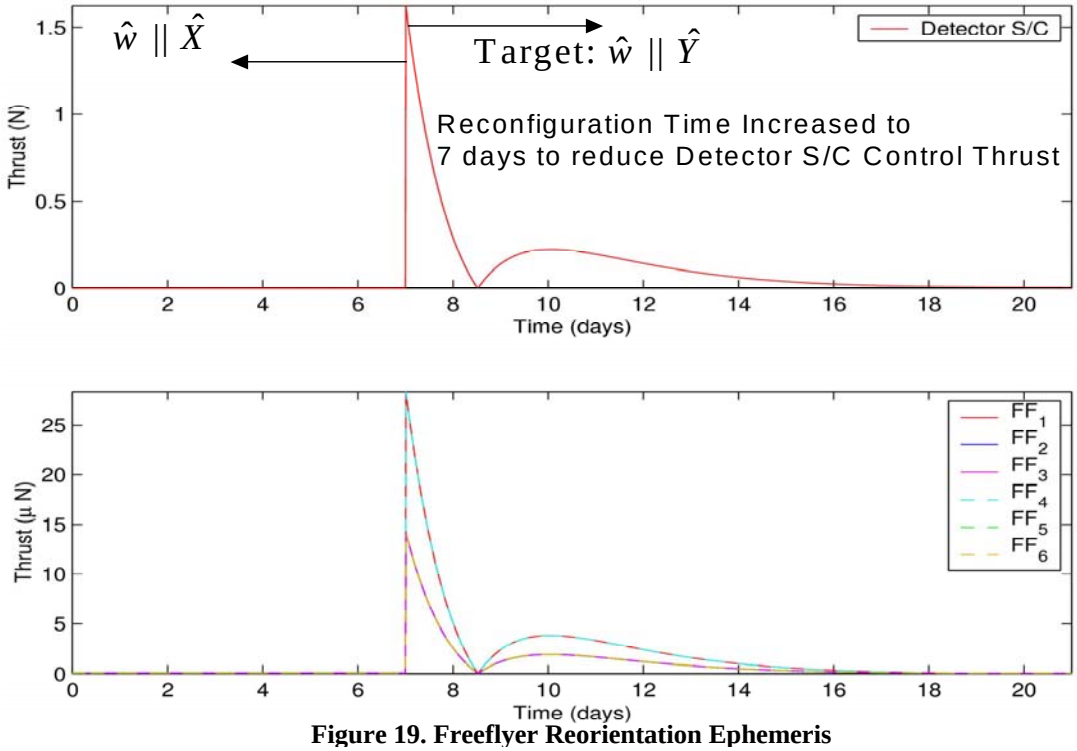


**Figure 19. Freeflyer Reorientation Ephemeris**

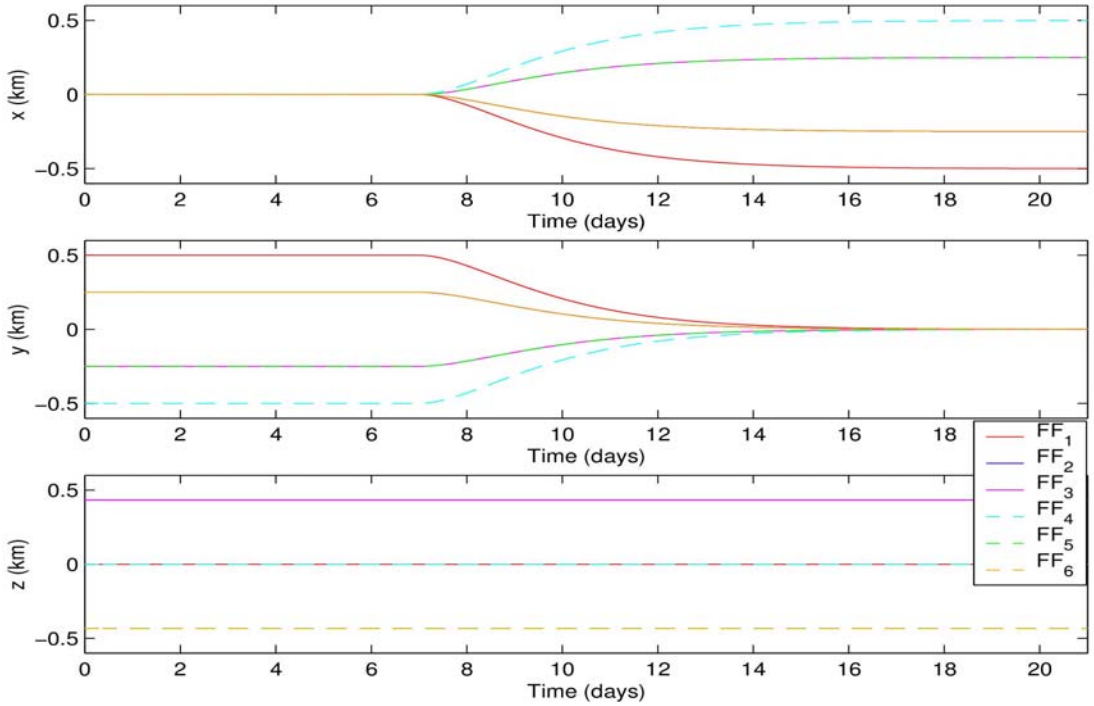


**Figure 20. Thrust Profile for Reorientation of 90 degrees**

## IV. Summary

Two approaches, discrete and continuous, were investigated for the control of the Maxim formation. It was found that control of the MAXIM formation can be accomplished using either discrete control with a simple or an optimal control strategy or by Input Feedback Linearization (IFL) control. To maintain the 5-micron tolerance on the freeflyer positions, the discrete control needs to operate at a time interval that approaches a continuous effort. An IFL was used which combines the effect of annihilating the environmental dynamics while adding a specific user-defined critically damped response to achieve the maintenance accuracy or to perform a recovery within a reasonable time.

The total effort of maintaining the nominal formation in the halo orbit requires a detector thrust level that ranges from 4 mN to 7 mN and freeflyer thrust levels of 0.1 μN to 0.3 μN. If allowed to drift, the science requirement of maintaining a five-micron position of the freeflyer in the optics plane is almost immediately violated, indicating the need for continuous thrusting. The thrust level for formation recovery after a reorientation ranges from between 0 to 1 N for the detector to less than a maximum of 15 μN for the freeflyers. These efforts do not include navigation or maneuver errors or navigation measurement updates.

## V. Conclusions

It was found that a continuous control effort is required to maintain the MAXIM formation requirements. The minimum thrust levels are at μN levels, which can be achieved by current propulsion technology. The challenge is whether a propulsion system can be implemented with control at the μN level and with the required power to maintain the formation if no allowable drift is permitted.

## VI. Acknowledgement

This work was supported by the revolutionary spacecraft systems project including cooperative agreement NCC5-727.

## VII. References

1. MAXIM web site, http://maxim.gsfc.nasa.gov.
2. MAXIM Proposal Response NRA 03-Oss-01-VM.
3. K. Gendreau et al., "Requirements and Options for a Stable Inertial Reference Frame for a 100 microarcsecond Imaging Telescope."
4. Y. Ulybyshev, "Long-Term Formation Keeping of Satellite Constellation Using Linear Quadratic Controller," *Journal of Guidance, Control, and Dynamics*, Vol. 21, No. 1, Jan.-Feb. 1998, pp.109-115.
5. D.J. Irvin Jr. and D.R. Jacques, "Linear vs. Nonlinear Control Techniques for the Reconfiguration of Satellite Formations," AIAA Guidance, Navigation, and Control Conference and Exhibit, Montreal, Canada, AIAA Paper 2001-4089. Aug. 6-9, 2001.
6. D.T. Stansbery and J.R. Cloutier, "Nonlinear Control of Satellite Formation Flight," AIAA Guidance, Navigation, and Control Conference and Exhibit, Denver, Colorado, AIAA Paper 2000-4436, Aug. 14-17, 2000.
7. S.R. Vadali, S.S. Vaddi, K. Naik, and K.T. Alfriend, "Control of Satellite Formations," *AIAA Guidance, Navigation, and Control Conference and Exhibit*, Montreal, Canada, Aug. 6-9, 2001. AIAA Paper 2001-4028.

8. H. Schaub and K. Alfriend, "Impulsive Spacecraft Formation Flying Control to Establish Specific Mean Orbit Elements," *Journal of Guidance, Control, and Dynamics*, Vol. 24, No. 4, July-Aug. 2001, pp. 739-745.
9. V. Kapila, M.S. de Queiroz, and Q. Yan, "Adaptive Nonlinear Control of Multiple S/C Formation Flying," *Journal of Guidance, Control, and Dynamics*, Vol. 23, No. 3, May-June 2000, pp. 385-390.
10. J. Lawton, R. W. Beard, F. Y. Hadaegh. An Adaptive Approach to Satellite Formation Flying With Relative Distance Constraints. Proceedings of the American Control Conference, June 1999, pp. 1545-1549.
11. D. J. Scheeres and N. X. Vinh, "Dynamics and Control of Relative Motion in an Unstable Orbit," AAS/AIAA Astrodynamics Specialists Conference, Denver, Colorado, AIAA Paper No. 2000-4135, Aug. 2000.
12. P. Gurfil and N.J. Kasdin, "Dyanmics and Control of Spacecraft Formation Flying in Three-Body Trajectories," AIAA Guidance, Navigation, and Control Conference and Exhibit, Montreal, Canada, Aug.6-9, 2001. AIAA Paper 2001-4026
13. B. Barden and K. Howell, "Fundamental Motions Near Collinear Libration Points and Their Transitions," *Journal of the Astronautical Sciences*, Vol 46. No. 4, Oct-Dec., 1998, pp. 361-378.
14. B. Barden and K. Howell, "Formation Flying in the Vicinity of the Libration Points," *Advances in the Astronautical Sciences*, Vol. 99, No. 2, 1998, pp. 969-988.
15. B.T. Barden and K.C. Howell, "Dynamical Issues Associated with Relative Configurations of Multiple Spacecraft Near the Sun-Earth/Moon $L_1$ Point," AAS/AIAA Astrodynamics Specialists Conference, Girdwood, Alaska, AAS Paper No. 99-450, Aug. 1999.
16. K.C. Howell and B.T. Barden, "Trajectory Design and Stationkeeping for Multiple Spacecraft in Formation Near the Sun-Earth $L_1$ Point," IAF 50$^{th}$ International Astronautical Congress, Amsterdam, Netherlands, IAF/IAA Paper 99-A707, Oct. 1999.
17. J. Masdemont, G. Gómez, M. Lo, and K. Museth, "Simulation of Formation Flight Near Lagrange Points for the TPF Mission," AAS/AIAA Astrodynamics Specialists Conference, Quebec, Canada. AAS Paper No. 01-305, Aug. 2001.
18. R. Luquette and R. Sanner,"A Non-Linear Approach for Spacecraft Formation Control in the Vicinity of a Collinear Libration Point." Proceeding of the AAS/AIAA, Astrodynamics Specialists Conference, Quebec, Canada, Aug. 2001, pp 437-445.
19. N. Hamilton and D. Folta, "Formation Flying Satellite Control Around the L2 Sun-Earth Libration Point," AAS/AIAA Astrodynamics Specialist Conference, Monterey, California, Aug. 2002.
20. K. Howell and B. Marchand, "Control Strategies for Formation Flight in the Vicinity of the Libration Points," AIAA/AAS Space Flight Mechanics Conference, Ponce, Puerto Rico, AAS Paper No.03-113, Feb. 2003.
21. B. Marchand and K. Howell, "Formation Flight Near L1 and L2 in the Sun-Earth/Moon Ephemeris System Including Solar Radiation Pressure," AAS/AIAA Astrodynamics Specialist Conference, Big Sky, Montana, AAS Paper No. 03-596, Aug. 2003.
22. B. Marchand and K. Howell, "Baseline Formations and the Associated Control Strategy near Halo Orbits," 2004 AAS/AIAA Space Flight Mechanics Conference, Maui, Hawaii, AAS Paper No. 04-157, Feb. 2004.